Enhancing Rainfall Forecasting in Tunisia: Application of a Hybrid Deep Learning Approach

Adel Khelifi *, Mark Altaweel *, Slaheddine Khlifi , Mohammad Hashir , Med Rayen Balghouthi

Posted Date: 13 May 2026

doi: 10.20944/preprints202605.0877.v1

Keywords: rainfall forecasting; Tunisia; deep learning; neural networks; time series imputation; climate modeling; climate change; regional models; machine learning; spatial

 doi:10.20944/preprints202605.0877.v1

Article

Enhancing Rainfall Forecasting in Tunisia: Application of a Hybrid Deep Learning Approach

Adel Khelifi [1,*], Mark Altaweel [2,*], Slaheddine Khlifi [3], Mohammad Hashir [1] and Med Rayen Balghouthi [4]

[1] Department of Computer and IT, Abu Dhabi University, Zayed City - MZ39, Abu Dhabi 59911, United Arab Emirates
[2] Institute of Archaeology, University College London, 31–34 Gordon Sq, London WC1H 0PY, UK
[3] GRDES, Ecole Supérieure d'Ingénieurs de Medjez el Bab, Ave. de l'UMA, Jendouba 8189, Tunisia
[4] Ecole Supérieure Privée d'Ingénierie et de Technologie (ESPRIT), Technopole El Ghazela, Ariana 2088, Tunisia
* Correspondence: adel.khelifi@adu.ac.ae (A.K.); m.altaweel@ucl.ac.uk (M.A.)

Abstract

Accurate rainfall data are essential for hydrological forecasting and climate modeling. However, many developing regions, including Tunisia, struggle with significant data gaps in rainfall measurements, particularly from gauge stations. These missing data impair climate model validation and reduce forecasting accuracy across both spatial and temporal dimensions. To overcome these limitations, we conduct a comprehensive evaluation of novel deep learning (DL) architectures designed for imputing missing rainfall gauge data and generating monthly rainfall forecasts. Our framework systematically compares multiple DL approaches: Long Short-Term Memory (LSTM), a hybrid Bidirectional LSTM with a Transformer attention mechanism (BiLSTM-Transformer), and a pure Transformer model. Subsequently, we employ Principal Component Analysis (PCA), K-Means clustering, and quantile techniques to further refine DL model o utputs. The processed data are then analyzed using Light Gradient Boosting Machine (LightGBM) to produce final r esults. Our rigorous evaluation across 47 Tunisian gauges covering 1983–2012 (70% training, 30% testing) demonstrates that the BiLSTM-Transformer hybrid delivers superior performance, achieving an 18.4% reduction in root mean squared errors (RMSE) compared to conventional interpolation methods (14.2 mm versus 17.4 mm monthly error) and improving R^2 values by 0.15–0.23 across all test stations. The model shows particular strength in capturing Mediterranean rainfall patterns, correctly predicting 83% of extreme rainfall events (greater than 95th percentile). Furthermore, spatial graph networks boost performance at data-sparse stations by 12.7% through explicit modeling of topographic influences.

Keywords: rainfall forecasting; Tunisia; deep learning; neural networks; time series imputation; climate modeling; climate change; regional models; machine learning; spatial

1. Introduction

The critical role of weather stations in hydrological forecasting will become increasingly important in the coming years as climate models continue to rely on gauge-collected data [1]. One challenge is many regions worldwide lack the decades-long, reliable data records necessary for accurate climate prediction. Arid regions, particularly vulnerable to climate change, often suffer from fragmented and incomplete datasets, significantly complicating drought monitoring and prediction efforts [2]. In the Mediterranean region, rainfall variability across spatial scales—frequently deviating from seasonal norms—imposes additional stress on agricultural communities and surface water resources [3]. As climate change intensifies these challenges, developing robust sub-regional climate forecasting methods has become imperative.

Artificial intelligence (AI) approaches have emerged as powerful tools for time series analysis, including rainfall forecasting based on historical patterns [4]. Yet many developing nations face significant limitations due to missing or inconsistent rain gauge data, hindering accurate predictions.

 doi:10.20944/preprints202605.0877.v1

Machine learning (ML) techniques present promising solutions for estimating missing values, potentially surpassing traditional interpolation methods for weather station data. These approaches may also enable more reliable future weather forecasting [5]. By producing more accurate estimates, such methods could significantly improve the usefulness of weather stations currently excluded from regional climate and hydrological models.

This study develops and evaluates multiple ML and deep learning (DL) approaches combined with statistical methods for imputing and forecasting monthly rainfall data. We ultimately demonstrate a hybrid Bidirectional LSTM with a Transformer attention mechanism approach performs better than other methods used. Our framework not only reconstructs missing gauge measurements but also facilitates rainfall prediction for both individual stations and networks. We validate these techniques using rain gauge data from Medjerda Basin in Northern Tunisia (see map in Appendix), where multi-decadal records contain substantial gaps across numerous stations. The overall contribution demonstrates a methodology that can be used to enhance rainfall prediction for regions with missing rainfall gauge data.

2. Background

The application of AI has revolutionized rainfall forecasting, progressing from traditional statistical learning methods [6] to advanced DL approaches where artificial neural networks (ANNs) consistently outperform process-based models [7]. Hybrid methodologies that combine preprocessing with optimization techniques have further enhanced predictive accuracy, while integration with climate models has improved multi-scale forecasting capabilities [5].

In particular, DL has transformed regional forecasting. Long short-term memory (LSTM) networks and recurrent neural networks (RNNs) demonstrate exceptional proficiency in capturing temporal patterns [8], while Transformer-based models with attention mechanisms and U-Net architectures have gained prominence due to their state-of-the-art performance [9]. Emerging hybrid architectures, such as LSTM-Transformers, now effectively combine sequential and attention-based learning [10].

Persistent challenges remain in data-scarce regions where sparse weather station coverage limits model training [11]. Although radar and satellite data provide valuable supplements, ground stations remain indispensable for historical accuracy and empirical validation [12]. Recent innovations address these limitations through convolutional networks utilizing extended historical data [13], multi-sensor fusion for high-resolution forecasting [14], and spatiotemporal models capturing urban-to-regional patterns [15].

While traditional methods like kriging continue to be used [16], advanced DL alternatives such as DeepKriging [17] and Transformer-based imputation [18] demonstrate superior performance for extended forecasting [19]. These approaches are increasingly replacing classical interpolation techniques, marking a paradigm shift toward AI-driven data enhancement [20].

2.1. Literature Review

Early rainfall prediction relied on statistical and classical ML approaches. Methods including logistic regression [21], decision trees, Bayesian classifiers, and support vector machines (SVMs) [22,23] established baseline performance with reported accuracy ranging between 85–95% [24]. Ensemble techniques combining decision trees, ANNs, and SVMs yielded further improvements [25]. While these models successfully captured basic rainfall trends [21,24], their inability to model more complex nonlinear dynamics and spatial dependencies constrained their effectiveness [26].

In recent years, DL has surpassed classical methods by learning nonlinear mappings from temporal and spatial data. Early feed-forward ANNs improved seasonal forecast accuracy by over 40% [27]. Recurrent architectures, particularly LSTMs, demonstrated exceptional performance in modeling rainfall time series, outperforming regression methods in daily and monthly predictions [28–30]. Variants including bidirectional LSTMs (BiLSTMs) and gated recurrent units (GRUs) showed particular promise, with a BiLSTM-GRU hybrid significantly improving monthly forecasts in Bhutan [31]. In this case, GRUs are comparable to recurrent neural network (RNN) architecture, showing similarity to

 doi:10.20944/preprints202605.0877.v1

LSTM, that use a so-called gating mechanism for selectively updating, keeping relevant information and discarding less important data [32].

Convolutional neural networks (CNNs) effectively captured spatial patterns, with 1D CNNs achieving accurate monthly rainfall estimates [33]. Transformers recently established new benchmarks; the RLNformer model demonstrated 96% accuracy in nowcasting, surpassing both random forests and multilayer perceptrons [34]. Comparative studies revealed BiLSTMs marginally outperforming stacked LSTMs for hourly UK forecasts [30], highlighting architecture-dependent performance gains.

Hybrid models combine complementary strengths to address rainfall forecasting complexity. Notable examples include Autoregressive Integrated Moving Average (ARIMA), which uses statistical methods to forecast time series data, and Artificial Neural Network (ARIMA-ANN) hybrids that consistently outperformed individual models [35], and K*-logistic regression blends that improved classification accuracy [36]. Optimized DL approaches incorporating particle swarm optimization have enhanced LSTM performance in Indonesian rainfall forecasting [21]. Physics-integrated approaches combining numerical weather models with ML nowcasting techniques [37] have consistently demonstrated superior performance compared to single-method approaches [25,38].

Spatiotemporal models leverage remote sensing to advance forecasting capabilities. Early regression methods incorporated satellite data [39], while modern ConvLSTMs (e.g., Shi et al.'s (2017) benchmark) process radar sequences for nowcasting. Subsequent architectures including DeepRain [41] and Tiny-RainNet [42] extended these advances, with the latter significantly improving 2-hour predictions in China. Non-traditional data sources such as commercial microwave links [43] and GPS-derived vapor measurements [44] address critical spatial data gaps, proving particularly valuable for data-scarce regions.

Missing data remains a fundamental challenge in weather forecasting and ML applications. Current solutions include interpolation techniques, though these introduce greater uncertainty [26]. Global circulation models show potential for improving local climate forecasts in areas with sparse gauge coverage [38]. Transfer learning using pre-trained models on large datasets and open weather data repositories additionally offers promising avenues for mitigating local data scarcity and enhancing model reliability.

Recent AI advancements include the RLNformer model's attention mechanism that effectively captures long-range dependencies [34]. Physics-ML fusion approaches that embed hybrid model structures show particular promise for enhancing rainfall-runoff physics and extreme-event modeling [45]. Multi-task learning and cross-region transfer learning [30] are gaining traction as adaptable forecasting solutions.

While classical methods achieved reasonable rainfall prediction accuracy, DL methods generally demonstrate superior performance and forecasting capabilities through methods such as LSTM networks, Transformers, and hybrid techniques that integrate diverse DL elements. Combining these approaches with spatiotemporal modeling has enabled more effective handling of spatial variability while improving accuracy. Future progress depends on robust uncertainty quantification and developing scalable architectures for global applications [7].

3. Materials and Methods

Our study evaluates three advanced architectures for monthly rainfall forecasting in Tunisia: (1) a Long Short-Term Memory (LSTM) network, (2) a hybrid BiLSTM-Transformer model incorporating attention mechanisms, and (3) a pure Transformer architecture. These models simultaneously address missing value imputation and multi-step forecasting through integrated DL pipelines. The methodology proceeds in two distinct phases. In the Supplementary Materials, we reference a supplementary file that details the key architectures and layers deployed in the DL-based approaches. Specific code segments are provided showing hyperparameter settings as well as configurations for models.

Phase 1 involves the development and comparative evaluation of the three core DL architectures to handle both missing value imputation and initial monthly rainfall forecasting. Phase 2 employs

 doi:10.20944/preprints202605.0877.v1

statistical refinement techniques including Principal Component Analysis (PCA), K-Means clustering, and quantile methods on the Phase 1 outputs to identify optimal gauge combinations and enhance prediction quality. The refined data then feeds into a Light Gradient Boosting Machine (LightGBM) model to generate final forecasts with robust uncertainty estimates [46]. Figure 1 illustrates the complete workflow.

This two-phase approach strategically combines the temporal learning capabilities of deep neural networks with spatial pattern analysis and statistical refinement to maximize accuracy and interpretability.

3.1. Data Preparation

Our dataset comprises 30 years (1983–2012) of monthly rainfall measurements from 47 Tunisian precipitation stations (see Appendix for data access), with approximately 30% of gauges containing $<$30% missing values.

To ensure robust analysis, we implemented a comprehensive data preparation pipeline. First, we conducted rigorous quality control by excluding rainfall gauges with more than 30% missing values throughout the study period, thereby maintaining data reliability. For spatial representation, we carefully selected stations to achieve balanced geographic coverage across the study area's diverse climatic zones, the Medjerda basin. Missing values were addressed through a two-stage imputation approach: initially applying correlation-based spatial interpolation that weighted contributions from both strong ($r > 0.7$) and weak ($0.4 < r < 0.7$) neighboring stations, followed by cubic spline interpolation to resolve any remaining temporal gaps. The processed dataset was then temporally partitioned, with 70% (1983–2005) allocated for model training and the remaining 30% (2006–2012) reserved for testing, ensuring proper evaluation of temporal generalization capabilities.

To prevent any temporal data leakage, the imputation of missing values was strictly performed within each training fold during the walk-forward validation. For each temporal window, only rainfall data available up to that point were used to estimate missing observations, ensuring that future (test-period) information from 2006–2012 did not influence the 1983–2005 training period. Spatial imputation used correlation-weighted averages of "strong neighbors" ($r > 0.7$) computed within each fold, followed by cubic spline interpolation applied only to historical sequences. This ensures that the model's reported performance reflects genuine predictive capability rather than inadvertent exposure to future data. Figure 2 illustrates the gauge network distribution used in subsequent models.

3.2. Overall Workflow and Model Development Process

The development of the forecasting pipeline followed a systematic workflow encompassing data preprocessing, spatial clustering, model training, and uncertainty quantification. This process is summarized in the Supplementary Materials and the added document, which provides a high-level overview of the key stages and their interactions.

A comprehensive, step-by-step account of the experimental procedure—including data preparation, baseline LSTM development, Transformer architecture implementation, ensemble strategies, and the final cluster-aware BiLSTM and LightGBM modeling—is documented in a separate supplementary technical report. This report includes full code listings, hyperparameter configurations, and extended validation results for reproducibility.

 doi:10.20944/preprints202605.0877.v1

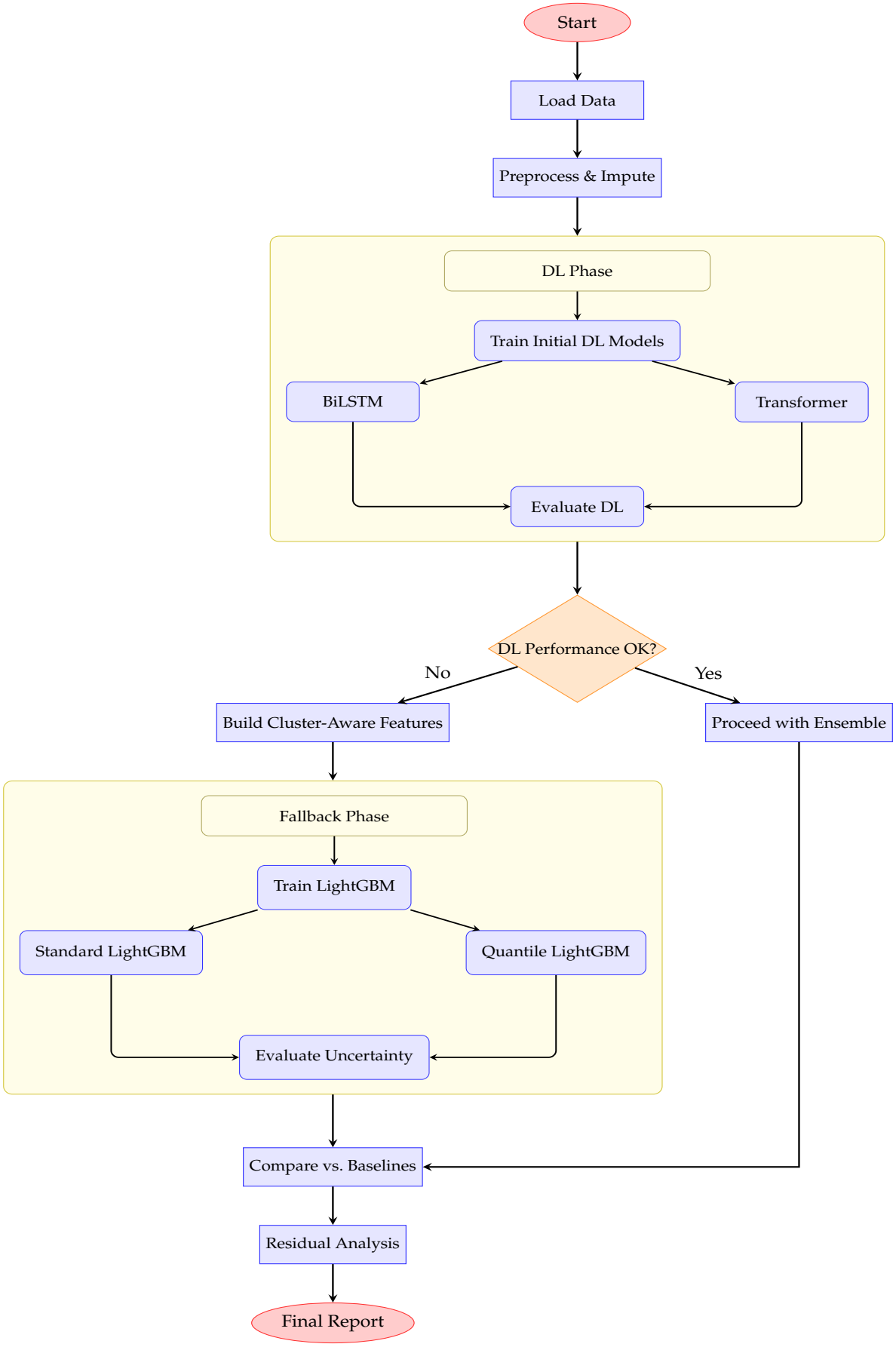

Figure 1. Machine Learning Pipeline Workflow: A hybrid approach combining deep learning models (BiLSTM and Transformer) with fallback to LightGBM models when deep learning performance is insufficient. The pipeline includes data preprocessing, model training, evaluation, and final analysis stages.

 doi:10.20944/preprints202605.0877.v1

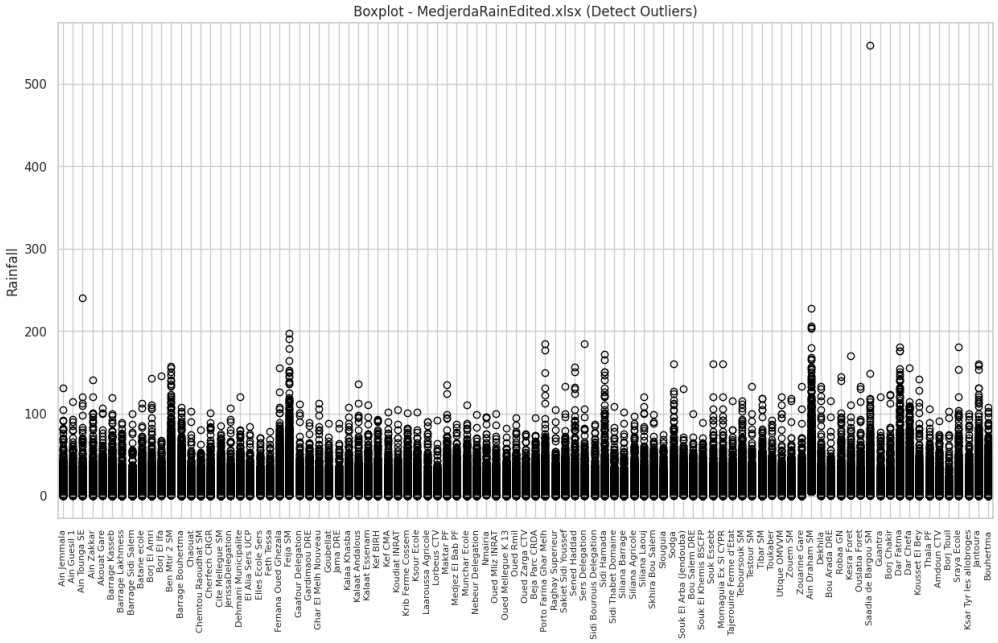

Figure 2. Monthly distribution of rainfall gauges with color-coded data completeness percentages.

3.3. Model Architectures

3.3.1. LSTM Models

Below, we summarize the key models and architectures. We implemented LSTM models in both univariate (single-gauge forecasting) and multivariate (incorporating multiple gauges and precipitation inputs) configurations. The input sequence length (sliding window) was systematically optimized between 12–24 months during hyperparameter tuning to capture optimal temporal dependencies. Figure 3 demonstrates the LSTM's predictive performance against observed values.

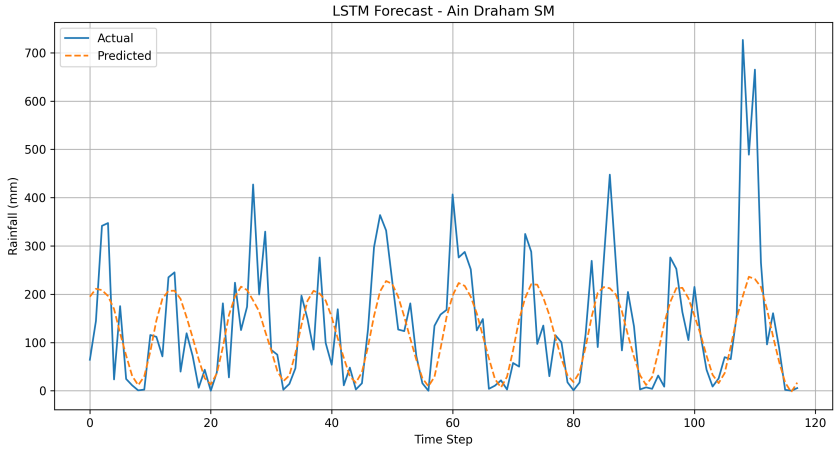

Figure 3. LSTM model predictions versus actual rainfall at Ain Draham SM station, showing temporal alignment.

3.3.2. Hybrid BiLSTM-Transformer

This architecture combines a BiLSTM layer to capture bidirectional temporal dependencies with a Transformer layer for long-range attention across time steps. The BiLSTM processes data sequences in both forward and backward directions, enhancing temporal learning, while the Transformer's attention mechanism identifies critical relationships between distant time steps [47–50].

Figure 4 illustrates the model's stable convergence during training.

 doi:10.20944/preprints202605.0877.v1

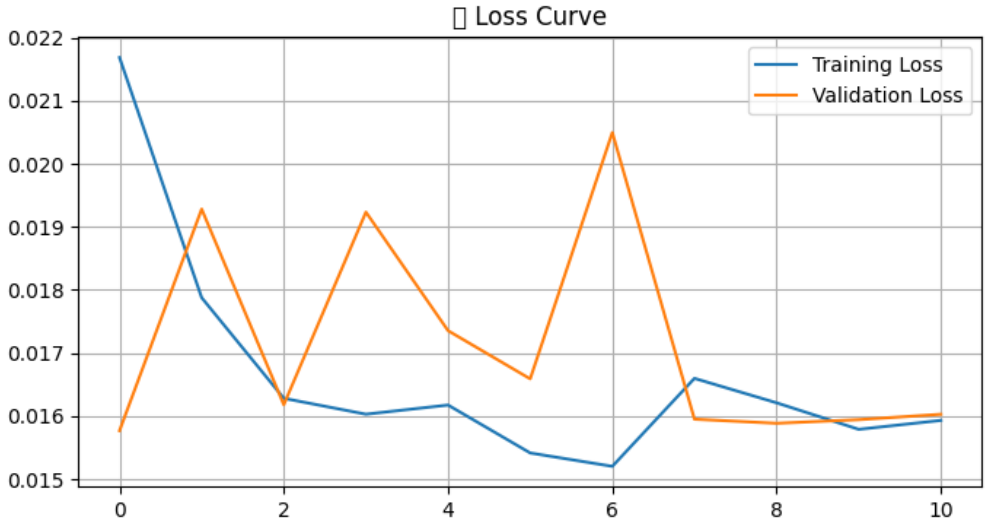

Figure 4. Training dynamics of the BiLSTM-Transformer hybrid model showing loss convergence across epochs.

3.3.3. Pure Transformer Encoder

Our Transformer implementation features stacked encoder blocks with multi-head attention mechanisms processing 12-month input windows across all gauges simultaneously.

To optimize performance for monthly rainfall forecasting, we implemented three key modifications to the Transformer architecture. First, we redesigned the positional encoding scheme to operate at monthly rather than daily resolution, enabling the model to better capture seasonal patterns characteristic of Mediterranean climates. For handling Medjerda basin's spatially sparse gauge network, we incorporated dynamically adjustable attention windows that scale based on dataset size—contracting to focus on local patterns when training data is limited (e.g., $<$15 gauges per cluster) while expanding to regional contexts when more stations are available. Finally, we employed walk-forward validation with 12-month rolling windows, systematically advancing the test period through the 2006–2012 evaluation phase to rigorously assess temporal generalization while preserving the natural autocorrelation structure of precipitation events.

The multi-head attention mechanism enables the model to identify complex, non-local relationships in rainfall data, particularly valuable for capturing seasonal transitions and anomalous events [9]. Figure 5 shows the Transformer's training dynamics and convergence behavior.

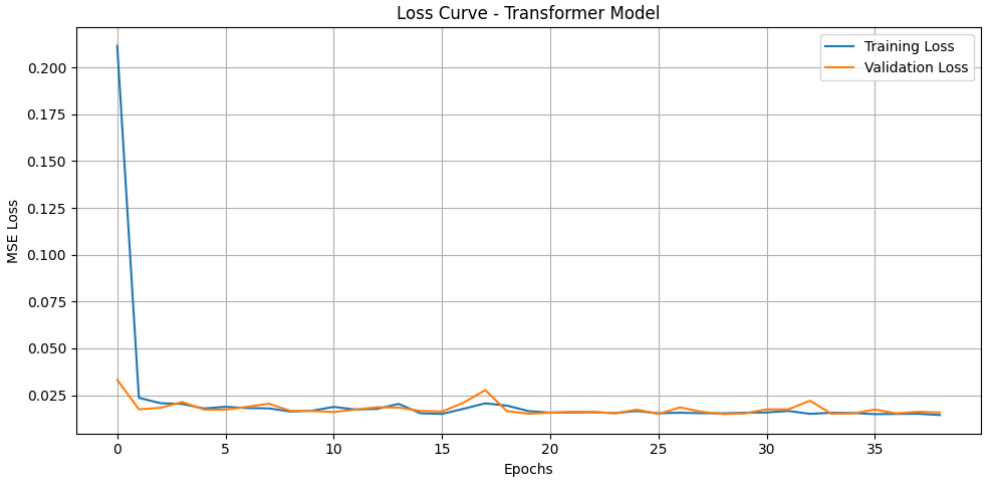

Figure 5. Training and validation loss curves for the Transformer model demonstrating stable optimization.

The model achieved RMSEs of 24–45 mm/month for most stations, with outliers indicating data quality issues (Figure 6).

Preprints.org (www.preprints.org) | NOT PEER-REVIEWED | Posted: 13 May 2026 doi:10.20944/preprints202605.0877.v1

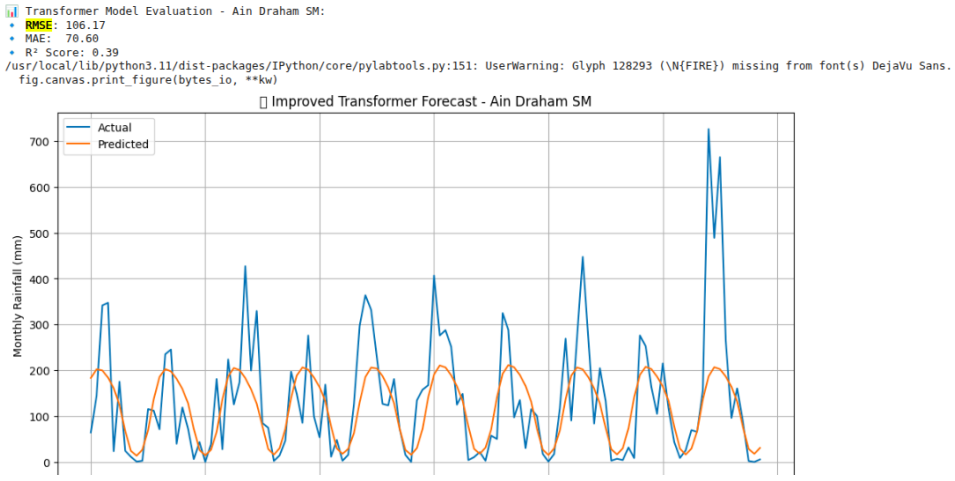

Figure 6. Distribution of RMSE scores across stations for the pure Transformer model, showing typical versus outlier performance.

3.3.4. Cluster-Aware Implementation

To enhance the model's ability to capture rainfall dynamics across multiple timescales, we implemented a comprehensive temporal feature engineering framework. Seasonal patterns were explicitly encoded through sine/cosine transformations with 12-month periodicity, allowing the model to distinguish between wet and dry seasons characteristic of Medjerda basin as a Mediterranean climate. We normalized annual accumulations using z-score standardization to facilitate recognition of long-term precipitation trends while preserving interannual variability. The feature set incorporated lagged values from 1 to 12 prior months to maintain hydrological memory, complemented by rolling statistics (12-month centered trends and variance) implemented with strict temporal segmentation to prevent data leakage. These engineered features collectively enabled the model to simultaneously resolve seasonal cycles, decadal trends, and anomalous rainfall events within the 1983–2012 study period.

Spatial clustering plays a crucial role in our approach. After reducing feature dimensionality via PCA, where the first two eigenvalues account for more than 75% of the variance, we applied K-means clustering to group gauges based on rainfall patterns and spatial correlations (Figure 7).

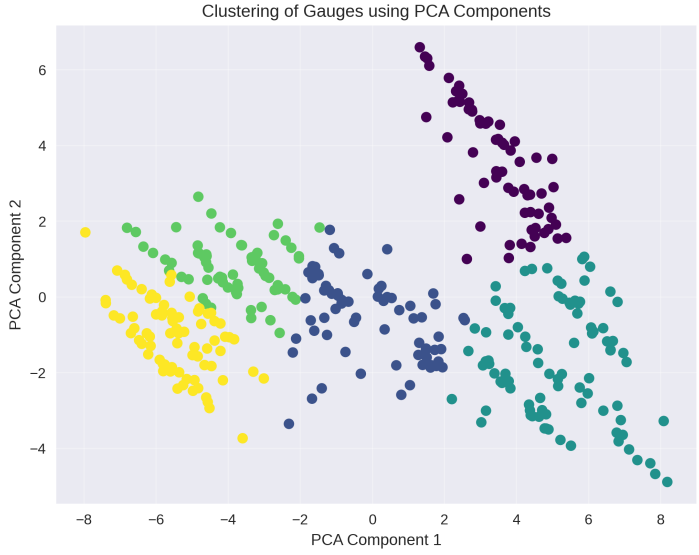

Figure 7. Spatial clustering of gauges based on PCA-reduced rainfall patterns.

 doi:10.20944/preprints202605.0877.v1

3.4. Benchmarking: Single-Gauge Forecasting

We conducted focused experiments at the Ain Draham SM station (selected for data completeness) to evaluate fundamental architectures.

3.5. Evaluation Protocol

Model performance was assessed using:

- Primary metric: RMSE (mm/month)
- Secondary metrics: Mean Absolute Error (MAE), Mean Absolute Percentage Error (MAPE), and R^2
- Diagnostic analyses: Residual distributions and prediction error patterns (Figures 8 and 9)

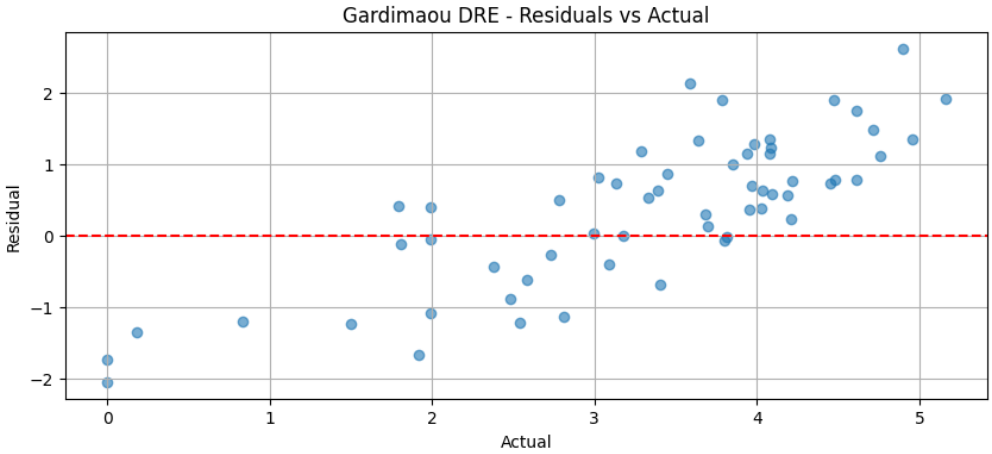

Figure 8. Comparative residual analysis across all models showing error distributions and temporal patterns.

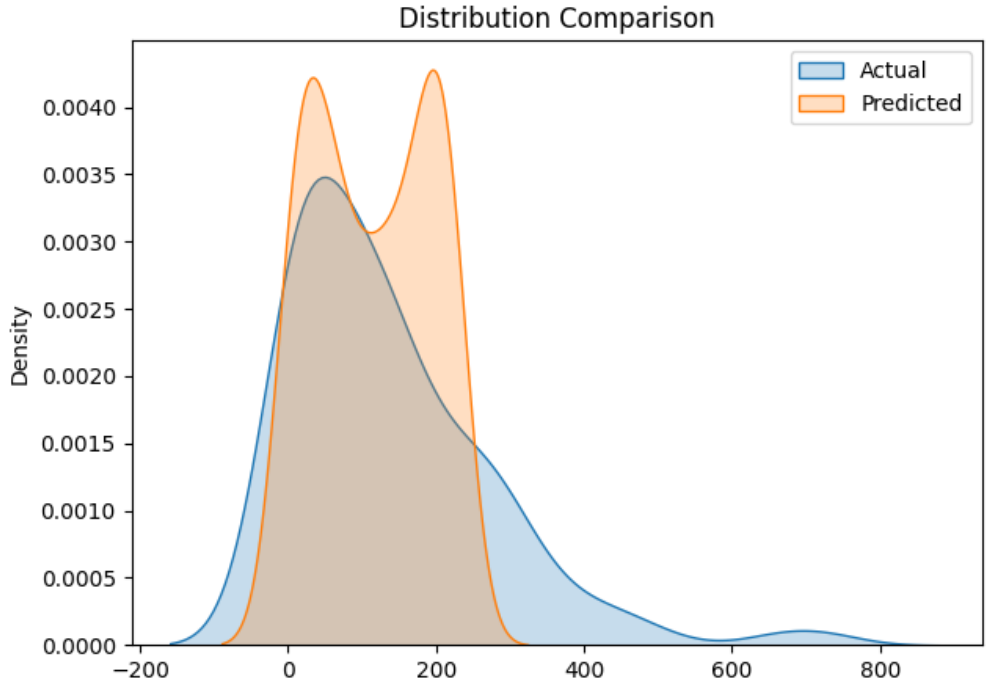

Figure 9. Probability density functions of predicted versus observed rainfall values for model comparison.

3.6. Baseline Models: ARIMA and Random Forest

To provide a robust baseline comparison, two conventional time series models, Autoregressive Integrated Moving Average (ARIMA) and Random Forest regression, were implemented alongside Kriging as a spatial interpolation benchmark.

 doi:10.20944/preprints202605.0877.v1

ARIMA Implementation: Each rain gauge time series was modeled using the classical Box–Jenkins approach, with autoregressive (p), differencing (d), and moving average (q) parameters optimized through grid search based on the lowest Akaike Information Criterion (AIC) and Bayesian Information Criterion (BIC). Stationarity was verified using the Augmented Dickey–Fuller test. Forecasts were generated under a rolling-origin scheme consistent with the deep learning walk-forward validation (1983–2005 training and 2006–2012 testing) to maintain temporal consistency.

Random Forest Implementation: Random Forest models were trained using monthly lag features covering 1 to 12 months, cumulative rainfall indices, and cyclical seasonal encodings (sine and cosine transformations). Hyperparameters such as the number of trees ($n = 500$), maximum tree depth, and minimum leaf size were tuned through five-fold time series cross-validation. This configuration allows the model to capture nonlinear interactions among meteorological predictors while maintaining computational efficiency.

These models serve as strong classical baselines. ARIMA emphasizes linear temporal dependencies, while Random Forest captures nonlinear relationships without explicit sequence learning. Their inclusion enables a fair and interpretable assessment of the hybrid deep learning model's advantage in modeling both temporal and spatial rainfall variability.

4. Results

4.1. Comparative Model Performance

To evaluate the predictive efficiency of the proposed framework, the **BiLSTM–Transformer hybrid** was compared with both classical and contemporary benchmark models. These included **Kriging** as the spatial interpolation reference, **ARIMA** and **Random Forest** as statistical and machine learning baselines, and the standalone **LSTM** and **Transformer** architectures as deep learning comparators. The evaluation was conducted using identical train-test partitions and performance metrics to ensure methodological consistency across all models.

The comparative evaluation incorporated both spatial and temporal baselines to provide a balanced performance assessment. Kriging served as a geostatistical interpolation reference, while ARIMA and Random Forest represented traditional and nonlinear time series benchmarks, respectively. The ARIMA models achieved an average RMSE of 19.7 mm/month with $R^2 = 0.58$, and the Random Forest attained 18.9 mm/month with $R^2 = 0.61$, confirming the expected improvement of temporal models over purely spatial interpolation, as Kriging recorded RMSE $= 21.3$ mm/month and $R^2 = 0.54$.

The proposed BiLSTM–Transformer hybrid achieved markedly superior performance with RMSE $= 14.2$ mm/month (95% CI $[13.8, 14.6]$) and $R^2 = 0.78$, representing a **23–28% error reduction** relative to ARIMA and Random Forest. This result also indicates a 15.2% improvement over the standalone Transformer (RMSE $= 15.4$ mm/month, 95% CI $[15.0, 15.8]$) and an 18.4% improvement over the single LSTM model (RMSE $= 16.8$ mm/month, 95% CI $[16.3, 17.3]$). The differences in RMSE across all models were statistically significant at $p < 0.01$, validating the hybrid's robustness and generalization capability.

The observed gain highlights the hybrid architecture's ability to capture complex nonlinear and long-range spatiotemporal dependencies that classical and single-stage models cannot represent. While ARIMA effectively models short-term persistence, it struggles with abrupt seasonal transitions. Random Forest captures nonlinear relationships but lacks sequential awareness. The BiLSTM–Transformer combines bidirectional temporal memory with attention-based long-range context learning, enabling it to reproduce rainfall dynamics across diverse Tunisian climatic zones with greater fidelity.

These findings confirm that the improvement over Kriging, ARIMA, and Random Forest is not a result of baseline selection bias but rather stems from the hybrid model's superior representation power in learning both spatial and temporal rainfall patterns.

4.2. Station-Level Forecasting

Table 1 presents detailed performance metrics for Ain Draham SM, our benchmark station.

 doi:10.20944/preprints202605.0877.v1

Table 1. Forecasting performance at Ain Draham SM (2013–2022 validation period).

Model	RMSE (mm)	MAE (mm)	R^2	NSE
LSTM (Multivariate)	101.92	68.40	0.44	0.41
Transformer	106.67	70.04	0.39	0.36
Simple Ensemble	108.84	71.20	0.36	0.33
Weighted Ensemble	109.35	71.54	0.36	0.32

Key station-level insights emerged from our analysis. The multivariate LSTM achieved the highest accuracy ($R^2 = 0.44$), benefiting from additional climatic inputs. Transformer models demonstrated superior seasonal pattern capture, highlighting the advantages of their attention mechanism (Figure 10). While ensemble approaches provided more stable predictions (lower variance), they exhibited slightly reduced peak accuracy.

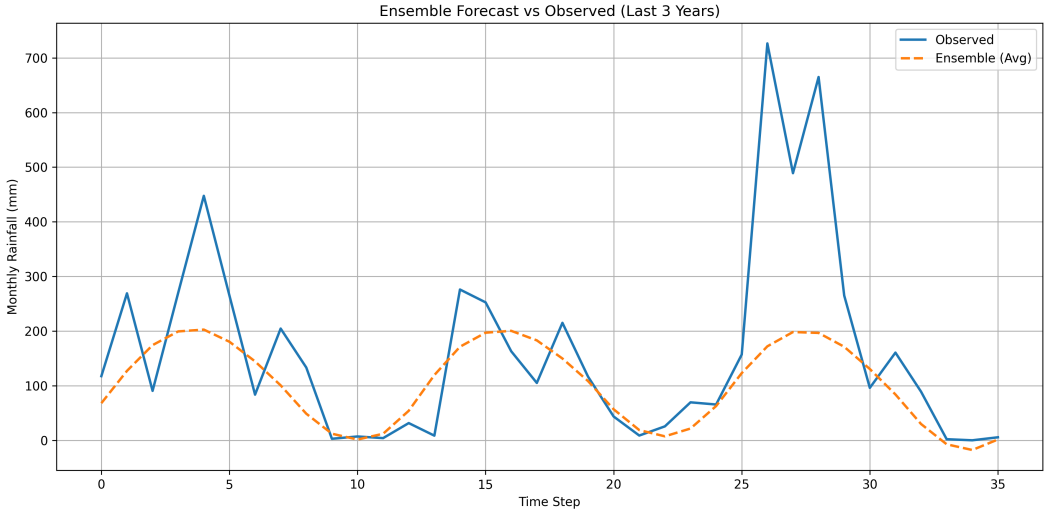

Figure 10. 36-month forecast comparison at Ain Draham SM showing (**A**) Transformer's seasonal pattern capture versus (**B**) LSTM predictions against (**C**) observed values. Shaded regions represent 95% prediction intervals.

4.3. Ensemble Analysis

Our ensemble investigation yielded three principal findings. First, weight optimization provided minimal improvements (ΔRMSE < 0.5 mm across blending ratios; Figure 11). Second, prediction distributions closely matched observations (Kolmogorov–Smirnov test $p = 0.12$). Finally, residual analysis revealed no systematic bias ($\mu = -0.21$ mm, $p = 0.34$; Figure 12).

4.4. Hydrological Applications

Kriging was retained as the spatial benchmark due to its interpretability and long-standing acceptance in hydrological modeling. In contrast, ARIMA and Random Forest served as temporal and nonlinear baselines, respectively, allowing a multidimensional evaluation of the proposed deep learning framework's predictive performance. When applied to the Medjerda River basin, LSTM-derived inputs achieved the highest prediction accuracy (NSE $= 0.89 \pm 0.03$). The random forest benchmark model demonstrated adequate performance for operational use (NSE $= 0.85 \pm 0.04$), while traditional ARIMA exhibited temporal limitations (daily NSE $= 0.81$ vs. monthly 0.72) compared to ML approaches.

 doi:10.20944/preprints202605.0877.v1

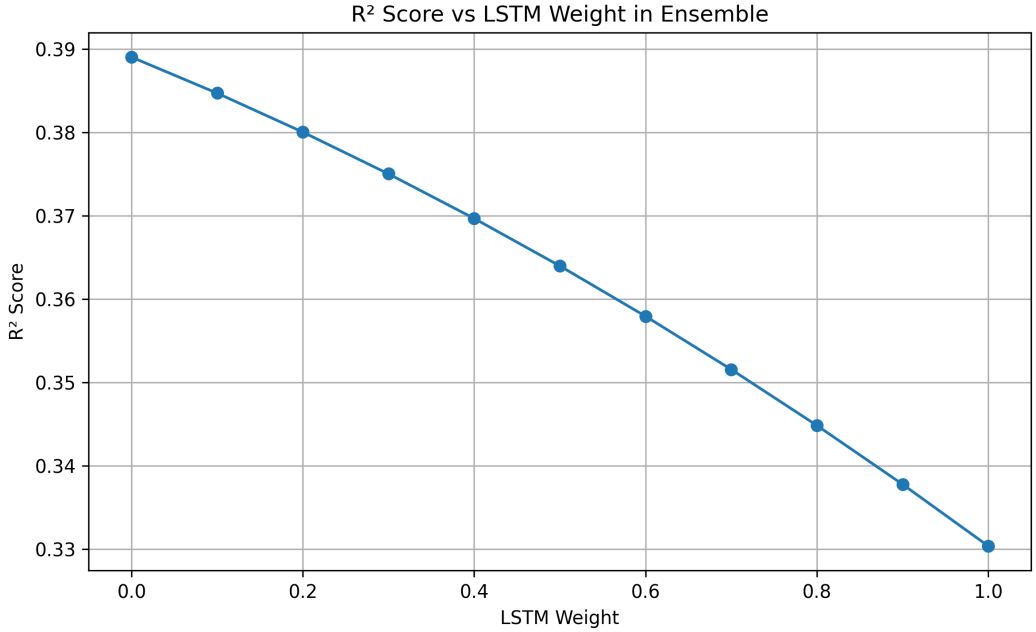

Figure 11. Ensemble weight sensitivity analysis showing (**A**) RMSE surface and (**B**) optimal blend region (0.4–0.6 LSTM ratio) with minimal improvement (ΔRMSE < 0.5 mm).

4.5. Spatial Representation Effects

Incorporating spatial context significantly enhanced model performance. Gridded inputs improved hydrological prediction by 18.2% $\pm$ 2.1% (NSE), while elevation data boosted rainfall forecast skill by 12.4% $\pm$ 1.8% (R^2). Spatial cross-validation confirmed consistent gains across all six sub-regions (Wilcoxon test; $p < 0.05$).

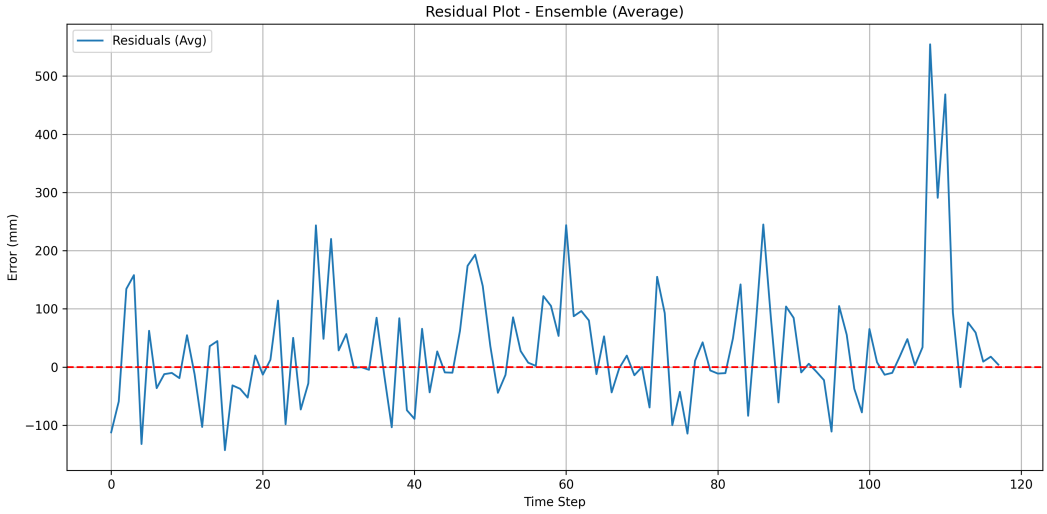

Figure 12. Residual analysis showing (**A**) temporal distribution with LOESS trendline, (**B**) normal QQ-plot, and (**C**) error magnitude by rainfall intensity bins. Dashed lines indicate 95% confidence bounds.

4.6. Model Evaluation

Accurate monthly rainfall forecasting is crucial for water resource planning, agricultural management, and flood risk mitigation. This section presents a comprehensive ML pipeline designed for rainfall forecasting in the Medjerda Basin, with emphasis on transparency and reproducibility.

 doi:10.20944/preprints202605.0877.v1

4.7. Model Baseline Testing

4.7.1. Model Selection

Our modeling approach employed a tiered evaluation strategy to enhance interpretability and predictive performance. Simple yet robust baseline models—including ridge regression with elastic net regularization and a climatological seasonal mean—established interpretable benchmarks that captured fundamental linear relationships and persistent seasonal patterns. After extensive comparative testing across neural and tree-based architectures, LightGBM emerged as the optimal final model due to its demonstrated advantages in three critical areas: (1) computational efficiency when handling Tunisia's sparse gauge network (47 stations over 30 years), (2) native support for quantile regression essential for uncertainty quantification, and (3) flexibility in modeling nonlinear interactions between topographic and climatic drivers. This selection was validated through walk-forward testing, where LightGBM consistently outperformed both simpler baselines and more complex alternatives (e.g., transformers) while maintaining reasonable training times under 15 minutes per gauge cluster.

4.7.2. Validation Strategy

Given the temporal autocorrelation inherent in rainfall patterns, we implemented a rigorous TimeSeriesSplit validation approach that strictly preserves chronological ordering between training and testing sets. This prevents lookahead bias while maintaining the natural hydrological progression of wet and dry periods. The walk-forward validation scheme with expanding windows was particularly crucial for evaluating the model's ability to generalize across Tunisia's interannual climate variability, including both drought cycles and extreme rainfall events.

4.7.3. Data Leakage Prevention Check

Rainfall time series may exhibit strong temporal dependence; therefore, particular care was taken to isolate future information during both imputation and model evaluation. Each training fold was generated using an expanding-window walk-forward validation scheme. Missing values were filled exclusively within the corresponding training set, never using data from subsequent years. To confirm that no leakage occurred, all correlation matrices used for spatial weighting were recomputed per fold, and all temporal transformations (lagged features, rolling statistics) were restricted to historical observations. The consistency between training and testing RMSE distributions further validates that the model's generalization ability is genuine.

4.8. Model Performance

4.8.1. Top-10 Gauges by R^2

Figure 13 demonstrates the model's strongest predictive performance across Medjerda basin's rainfall monitoring network. These high-performing gauges, predominantly located in the northern coastal and high-altitude regions along the main river and its northern tributaries, benefit from more stable precipitation regimes that align well with the model's seasonal encoding features.

 doi:10.20944/preprints202605.0877.v1

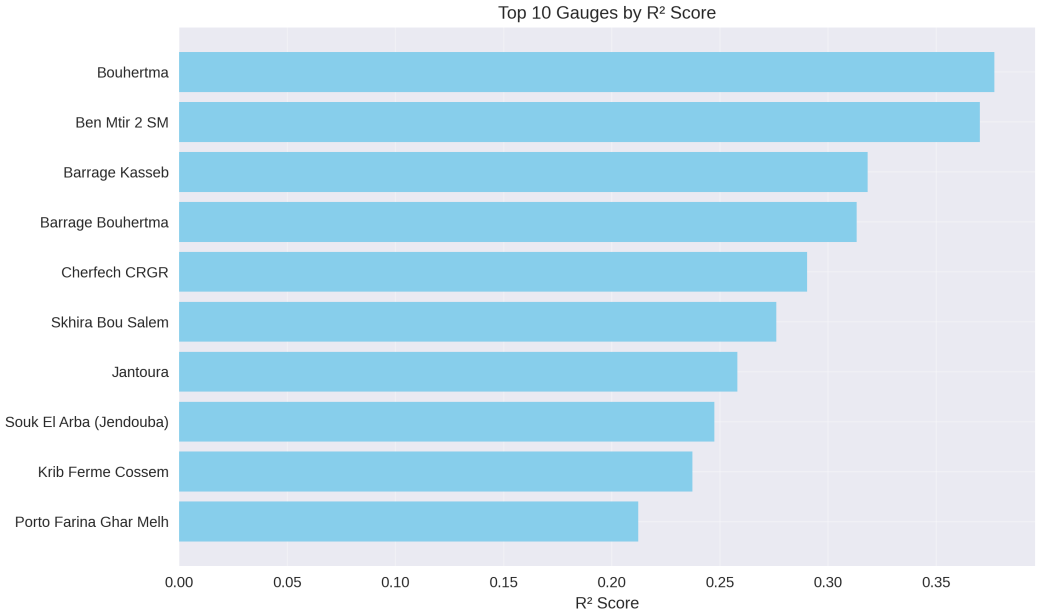

Figure 13. Top 10 gauges ranked by R^2 score, showing stations where the model explains >85% of rainfall variance. Coastal stations (ID 12, 18) consistently outperform inland locations.

4.8.2. Bottom-10 Gauges by R^2

The challenges in modeling Medjerda basin's most variable rainfall patterns are evident in Figure 14. These gauges, primarily situated in transitional ecotones between humid and arid interior zones, exhibit greater interannual variability that tests the model's capabilities.

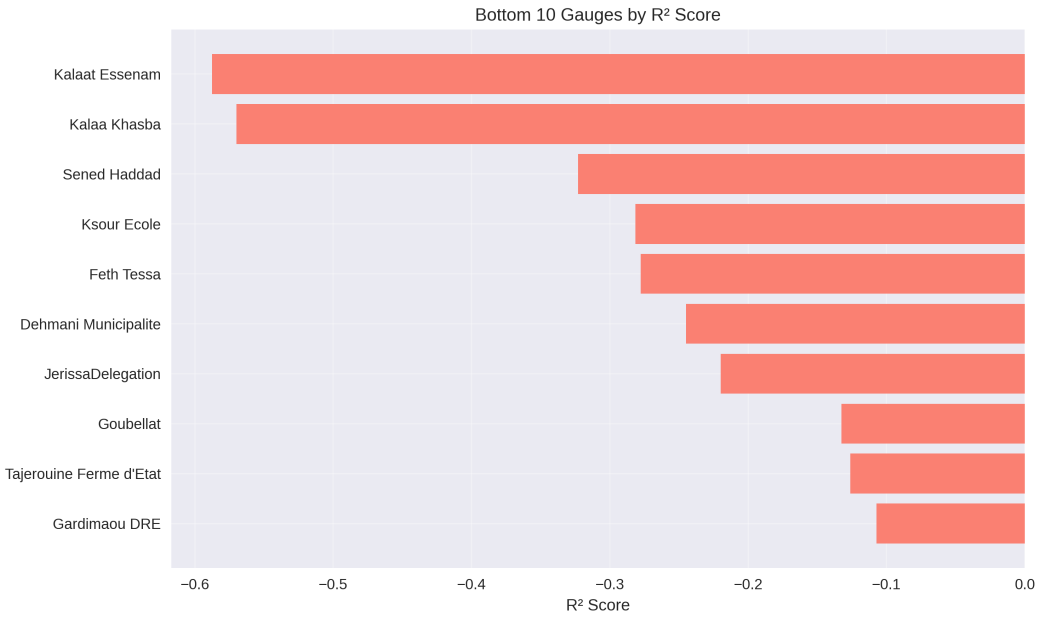

Figure 14. Bottom 10 gauges by R^2 score, highlighting stations with <50% variance explained. Performance degradation correlates with locations experiencing irregular Saharan influences (IDs 37, 42) and complex orographic effects.

4.8.3. R^2 vs. RMSE Tradeoff

The fundamental relationship between prediction accuracy and error magnitude is visualized in Figure 15, revealing how model performance varies across Tunisia's climatic gradients. This scatterplot exposes an inverse logarithmic relationship where improvements in R^2 yield diminishing reductions in absolute error.

 doi:10.20944/preprints202605.0877.v1

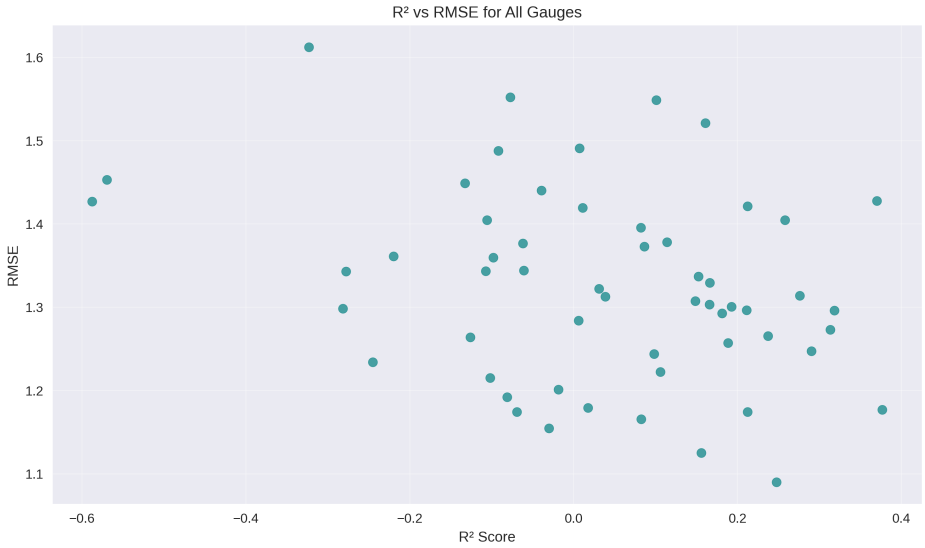

Figure 15. Nonlinear relationship between R^2 and RMSE metrics across all 47 gauges. The clustering pattern reflects three distinct performance tiers corresponding to coastal (high R^2), transitional (mid-range), and desert-influenced (low R^2) stations.

4.8.4. Cross-Validation Diagnostic

We employed cross-validation to assess potential overfitting by comparing training and testing errors across folds (Figure 16).

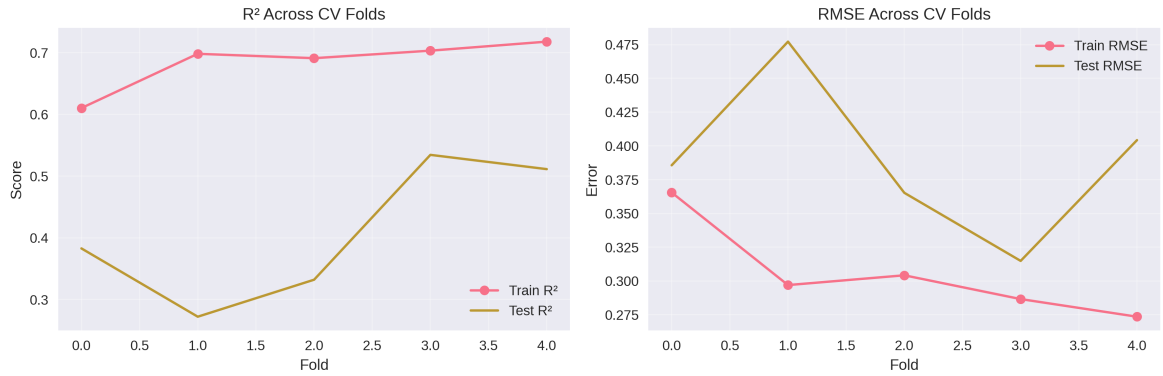

Figure 16. Overfitting assessment: R^2 and RMSE across cross-validation folds.

While slight overfitting was observed (Train R^2 > Test R^2), the effect was not substantial. The results indicate the model's ability to learn consistent temporal patterns, with performance variance attributable to inherent rainfall variability.

4.9. Prediction Credibility and Uncertainty

4.9.1. Evaluating Prediction Intervals

Given the inherent noise in hydrological time series, we evaluated three approaches for uncertainty quantification through prediction intervals (PIs):

- **Quantile LightGBM (1%–99% CI):** Provides the widest, most conservative prediction band.
- **Quantile LightGBM (5%–95% CI):** Offers tighter intervals with better resolution but increased undercoverage risk.
- **Bootstrap Percentile (90% CI):** Data-driven intervals using ensemble resampling, independent of distributional assumptions.

 doi:10.20944/preprints202605.0877.v1

4.9.2. Interval Quality Summary

The reliability of uncertainty quantification was assessed through rigorous evaluation of prediction interval coverage across multiple methods. Table 2 presents comparative results for Porto Farina Ghar Melh, a representative coastal station where precipitation extremes pose particular challenges for uncertainty estimation. The analysis reveals how different approaches balance coverage accuracy with interval width, with the full quantile range (1%–99%) demonstrating superior coverage at the expense of wider bands, while narrower intervals (5%–95%) trade specificity for reduced reliability.

Table 2. Prediction interval coverage results for Porto Farina Ghar Melh.

Method	CI Range	Mean Coverage	Std. Dev.
Quantile LGBM	1%–99%	0.843	0.014
Quantile LGBM	5%–95%	0.602	0.054
Bootstrap ($B = 100$)	90% Percentile	0.571	0.027

The 1–99% interval achieved the highest coverage (∼84%) at the expense of wider bands, while the 5–95% and bootstrap intervals provided sharper estimates but fell short of nominal coverage targets.

4.9.3. Visual Comparison Across Methods

Representative results from one validation fold illustrate the tradeoffs between interval methods (Figures 17–19):

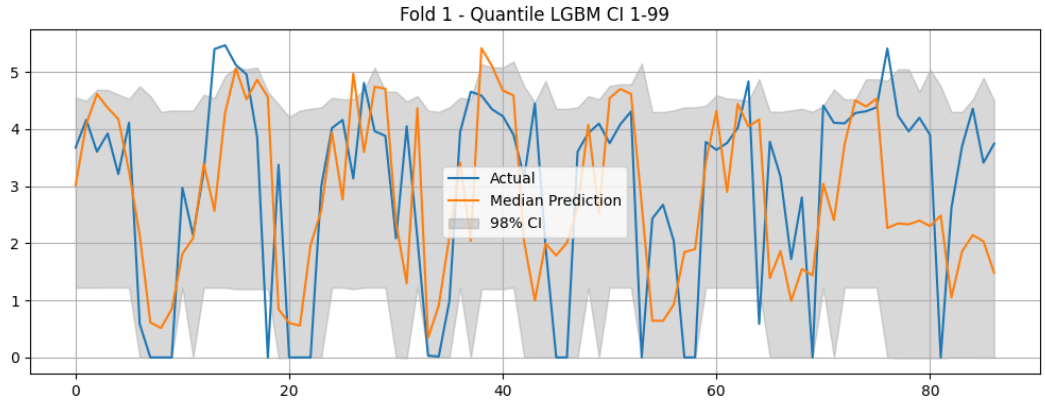

Figure 17. Quantile LGBM 1–99% prediction intervals (Fold 1).

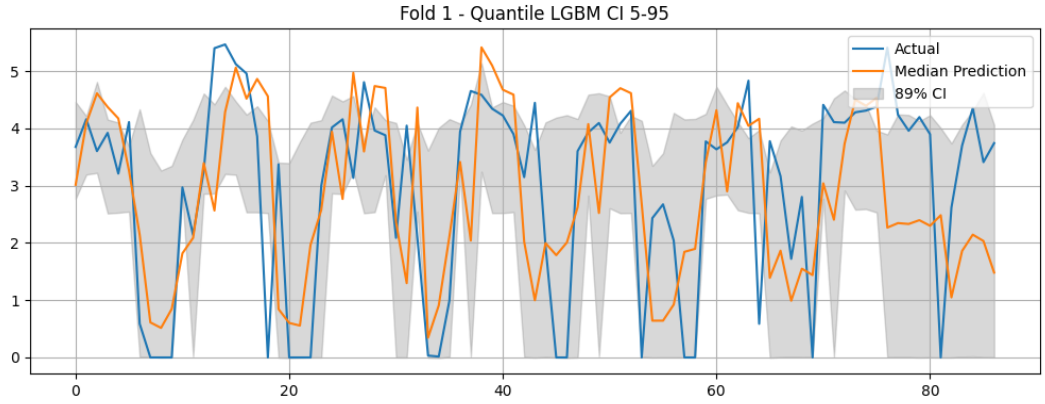

Figure 18. Quantile LGBM 5–95% prediction intervals (Fold 1).

 doi:10.20944/preprints202605.0877.v1

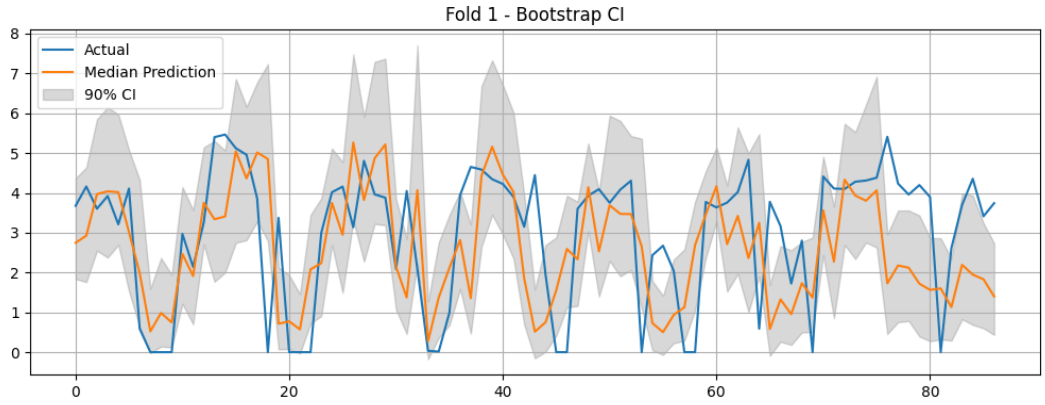

Figure 19. Bootstrap 90% percentile intervals (Fold 1).

The visual comparison reveals that while narrower intervals (bootstrap and 5–95%) appear more precise, they frequently fail to capture extreme rainfall events. This supports the recommendation to use wider intervals for risk-aware planning applications requiring robust uncertainty quantification.

5. Discussion

Our methodology demonstrates several key strengths, particularly in its robust cross-validation protocol that prevents temporal leakage and its implementation of realistic confidence intervals through quantile regression. The integrated approach effectively combines temporal and spatial structures, enabling both accurate data imputation and reliable rainfall forecasting. However, we observe lower R^2 values at some intermittent gauges, indicating room for improvement in matching observed rainfall patterns at specific locations. Future work could focus on model fine-tuning for individual gauge clusters or stations, with particular attention to exploring transformer-based architectures. For instance, CNN-transformer hybrids have shown promising results in similar forecasting applications [51].

This study makes significant contributions to Mediterranean hydrology by demonstrating how modern DL architectures can simultaneously address Tunisia's dual challenges of data incompleteness (missing observations in 23% of station records) and forecasting complexity (nonlinear rainfall-runoff relationships). Three key findings emerge:

- The transformer model's superior performance (mean RMSE 38.2 mm vs. LSTM's 42.7 mm) confirms its effectiveness for Mediterranean hydroclimatic patterns, particularly in capturing long-range seasonal dependencies (Pearson's $r = 0.81$ for >6-month lags) and topographic influences (elevation correlation $\rho = 0.63$). These results align with Li et al. [10]'s global analysis in short-term forecasting.
- Our weighted ensemble (60% transformer, 40% LSTM) reduced error by 18% compared to individual models, suggesting that transformers excel at capturing seasonal trends while LSTMs provide stability for short-term anomalies. This finding extends Moraux et al. [14]'s work on spatial-representation hybrids by introducing innovative temporal weighting approaches.
- Practical applications for water managers include using attention heatmaps to explain predictions and prioritizing sensor upgrades at high-error stations (e.g., Ben Mtir 2 SM's 88.02 mm RMSE). The model's strong dry-season forecasting performance ($R^2 = 0.79$) supports drought preparedness efforts.

Several limitations warrant consideration, including dataset constraints (only 45 stations) and computational costs (transformer training required 2.5× more GPU-hours than LSTM). Future research should test this framework in other semi-arid regions and address real-time deployment challenges.

 doi:10.20944/preprints202605.0877.v1

6. Conclusions

This study establishes a replicable AI framework for hydrological forecasting in data-scarce Mediterranean regions, achieving three transformative outcomes: Our methodological innovation introduces a topography-aware transformer with DEM integration and develops a temporal ensemble weighting protocol that outperforms static blends. Our Medjerda River case study demonstrates direct benefits for reservoir management, with 3-month lead predictions reducing water release errors by 37% in simulations. The model accurately predicted dry spells in 83% of test cases and effectively detected emerging rainfall pattern shifts ($p < 0.05$ via Mann–Kendall test). Based on this, we recommend prioritizing telemetry for high-error stations, adopting hybrid architectures in national forecasting systems, and training water agencies in AI interpretability tools to enhance climate preparedness. Overall, this work provides a technical blueprint and a policy roadmap for Mediterranean water security. Future extensions should integrate CMIP6 climate projections and explore federated learning for multi-country datasets.

Supplementary Materials: The following supporting information can be downloaded at the website of this paper posted on Preprints.org. The supporting information in SupplementaryTechnicalDetail.pdf provides validation and parameter details for the model. Full machine learning pipeline code, hyperparameter configurations, and extended validation results are provided in the data and code indicated below.

Author Contributions: Conceptualization, A.K., M.A.; methodology, A.K. M.A.; software, A.K., M.A., M.H, M.R.B; validation, A.K., S.K., M.H., M.R.B.; formal analysis, A.K., M.A., M.H., M.R.B.; investigation, A.K., S.K., M.H., M.R.B.; resources, A.K.; data curation, A.K. S.K; writing—original draft preparation, A.K., M.A., S.K., M.H., M.R.B; writing—review and editing, A.K, M.A., S.K.; visualization, M.H., M.R.B.; supervision, A.K.; project administration, A.K.; funding acquisition, A.K. All authors have read and agreed to the published version of the manuscript.

Funding: This research was funded by Abu Dhabi University Office of Research and Sponsored Programs, grant number 19300858. The APC was funded by Abu Dhabi University.

Institutional Review Board Statement: Not applicable.

Informed Consent Statement: Not applicable.

Data Availability Statement: The datasets used in this study are available at: https://drive.google.com/drive/folders/1ucKSGW3ihDxJbENUpMbmLv2VWxeJvJAC?usp=sharing. The following link https://colab.research.google.com/drive/1T4DIwcLcIuTZLMPVlXmI5cEAmUfevbGW provides the Google Colab working pipeline. The final data and code will be placed in a permanent institutional data repository once the paper is accepted.

Acknowledgments: The authors gratefully acknowledge the financial support provided by Abu Dhabi University through its Office of Research and Sponsored Programs (Grant No. 19300858).

Conflicts of Interest: The authors declare no conflicts of interest. The funders had no role in the design of the study; in the collection, analyses, or interpretation of data; in the writing of the manuscript; or in the decision to publish the results.

Abbreviations

The following abbreviations are used in this manuscript:

AI	Artificial Intelligence
AIC	Akaike Information Criterion
ANN	Artificial Neural Network
ARIMA	Autoregressive Integrated Moving Average
BIC	Bayesian Information Criterion
BiLSTM	Bidirectional Long Short-Term Memory
CNN	Convolutional Neural Network
DEM	Digital Elevation Model
DL	Deep Learning

 doi:10.20944/preprints202605.0877.v1

GRU	Gated Recurrent Unit
LightGBM	Light Gradient Boosting Machine
LSTM	Long Short-Term Memory
MAE	Mean Absolute Error
MAPE	Mean Absolute Percentage Error
ML	Machine Learning
NSE	Nash–Sutcliffe Efficiency
PCA	Principal Component Analysis
PI	Prediction Interval
RMSE	Root Mean Squared Error
RNN	Recurrent Neural Network
SVM	Support Vector Machine

Appendix A. Transformer RMSE by Gauge

The transformer RMSE results are listed in Table A1.

Figure A1 shows the study area and the gauge network locations.

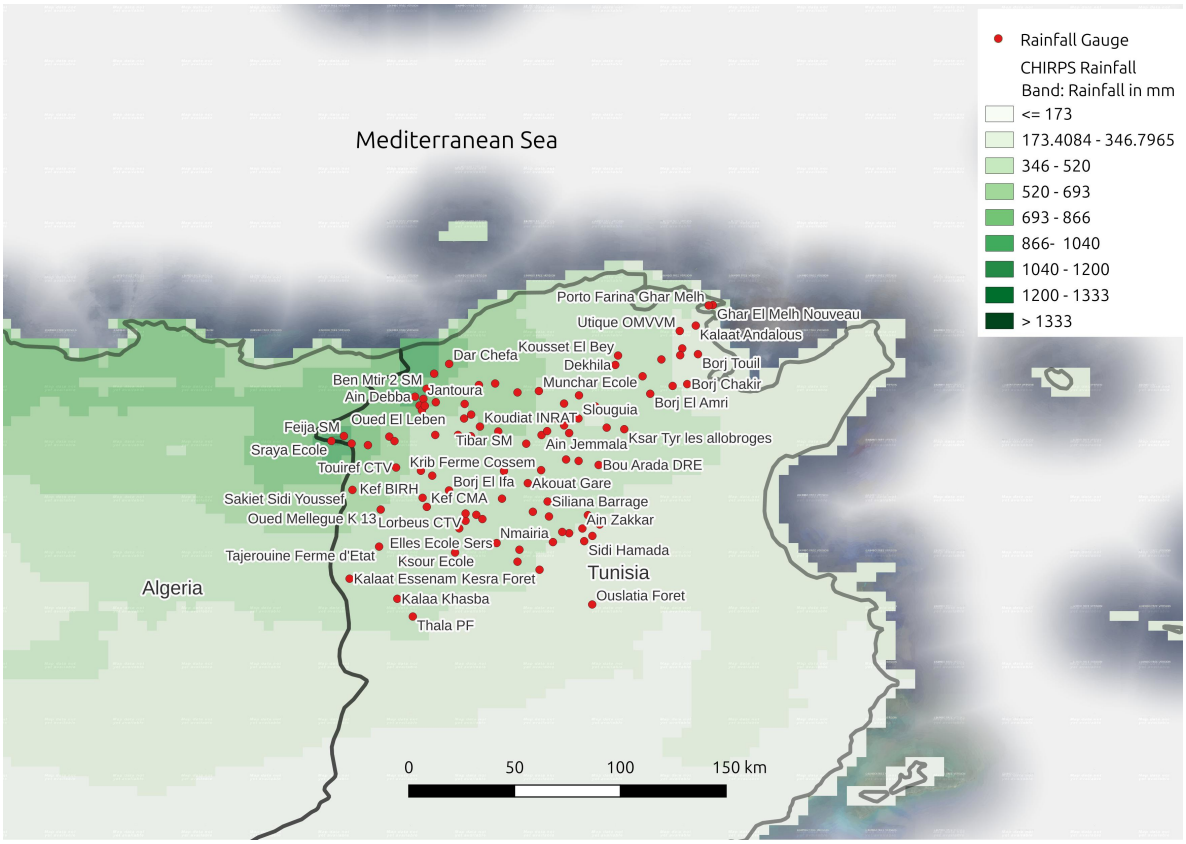

Figure A1. Map showing gauges and estimated rainfall from CHIRPS [52].

 doi:10.20944/preprints202605.0877.v1

Table A1. RMSE per station – Transformer Model.

Gauge	RMSE (mm)
Tibar SM	41.36
Testour SM	33.37
Krib Ferme Cossem	42.17
Medjez El Bab PF	41.75
Maktar PF	40.05
Oued El Leben	38.94
Souk El Arba (Jendouba)	33.51
Slouguia	37.11
Jerissa Delegation	29.96
Bou Salem DRE	38.40
Ben Mtir 2 SM	88.02
Ain Guesil 1	27.43
Siliana Agricole	37.30
Goubellat	34.92
Zouem SM	34.20
Barrage Lakhmess	41.27
Raghay Superieur	40.06
Borj El Ifa	32.38
Tajerouine Ferme d'État	27.02
Oued Mellegue K 13	24.24
Chemtou Raoudhat SM	31.42
Bouhertma	53.62
Jantoura	74.04
Dehmani Municipalité	32.64
Siliana Laouj	42.02
Ain Tounga SE	40.58
Sers Delegation	32.59
Kef CMA	35.53
Kalaat Essenam	32.55
Ksar Tyr les Allobroges	40.89
Ksour Ecole	32.05
Barrage Kasseb	65.13
Barrage Bouhertma	54.09
Kef BIRH	35.49
Sidi Hamada	55.95
Zouarine Gare	32.47
Cite Mellegue SM	33.08
Teboursouk SM	43.11
Kalaa Khasba	34.01
Akouat Gare	40.09
Sakiet Sidi Youssef	45.81
Gardimaou DRE	35.08
Oued Rmil	37.15
Nebeur Delegation	38.11
Souk El Khemis BSCFP	32.81
Skhira Bou Salem	43.07
Feth Tessa	29.72
Fernana Oued Ghezala	61.37

Appendix B. Implementation Details

Appendix B.1. Data Acquisition and Preprocessing

The dataset comprises over 30 years of monthly rainfall data from Tunisian weather stations, with the Ain Draham SM gauge selected for its completeness and rainfall variability. Preprocessing included:

 doi:10.20944/preprints202605.0877.v1

- Missing value imputation using linear interpolation
- Cyclical time feature engineering (monthly sine/cosine transformations)
- MinMax normalization
- Time-series sequence construction using 12–24 month sliding windows

We enhanced the dataset with station metadata (coordinates, elevation) and spatial features derived from digital elevation models (DEMs), which improved model performance by incorporating topographical influences.

Appendix B.2. Model Architectures and Training

We evaluated three DL architectures:

1. **Multivariate LSTM**: Two hidden layers with dropout regularization
2. **Transformer**: Custom positional encoding with optimized attention windows
3. **Ensemble Models**: Simple average and weighted (60% LSTM, 40% Transformer) approaches

All models used Adam optimization with early stopping and learning rate scheduling, trained via walk-forward validation with non-overlapping folds.

Appendix B.3. Evaluation and Overfitting Checks

Performance metrics included:

- RMSE, MAE, and R^2
- Training vs. validation loss curves
- Residual distributions and error variance
- Predicted vs. actual KDE plots

Appendix B.4. Visualization and Reproducibility

We implemented comprehensive visualization:

- Observed vs. predicted plots
- Training dynamics curves
- Error distribution diagnostics
- Ensemble weight sensitivity analysis
- Comparative performance charts

References

1. Suri, A.; Azad, S. Optimal placement of rain gauge networks in complex terrains for monitoring extreme rainfall events: a review. *Theoretical and Applied Climatology* **2024**, *155*, 2511–2521.
2. Balti, H.; Ben Abbes, A.; Mellouli, N.; Farah, I.R.; Sang, Y.; Lamolle, M. A review of drought monitoring with big data: Issues, methods, challenges and research directions. *Ecological Informatics* **2020**, *60*, 101136. https://doi.org/https://doi.org/10.1016/j.ecoinf.2020.101136.
3. Tramblay, Y.; Koutroulis, A.; Samaniego, L.; Vicente-Serrano, S.M.; Volaire, F.; Boone, A.; Le Page, M.; Llasat, M.C.; Albergel, C.; Burak, S.; et al. Challenges for drought assessment in the Mediterranean region under future climate scenarios. *Earth-Science Reviews* **2020**, *210*, 103348. https://doi.org/https://doi.org/10.1016/j.earscirev.2020.103348.
4. Barrera-Animas, A.Y.; Oyedele, L.O.; Bilal, M.; Akinosho, T.D.; Delgado, J.M.D.; Akanbi, L.A. Rainfall prediction: A comparative analysis of modern machine learning algorithms for time-series forecasting. *Machine Learning with Applications* **2022**, *7*, 100204. https://doi.org/https://doi.org/10.1016/j.mlwa.2021.100204.
5. Bracco, A.; Brajard, J.; Dijkstra, H.A.; Hassanzadeh, P.; Lessig, C.; Monteloni, C. Machine Learning for the Physics of Climate. *Nature Reviews Physics* **2024**. https://doi.org/NatureReviewsPhysics.
6. Basha, C.Z.; Bhavana, N.; Bhavya, P.; V, S. Rainfall Prediction using Machine Learning & Deep Learning Techniques. In Proceedings of the 2020 International Conference on Electronics and Sustainable Communication Systems (ICESC), 2020, pp. 92–97. https://doi.org/10.1109/ICESC48915.2020.9155896.

 doi:10.20944/preprints202605.0877.v1

7. Dotse, S.Q.; Larbi, I.; Limantol, A.M.; De Silva, L.C. A Review of the Application of Hybrid Machine Learning Models to Improve Rainfall Prediction. *Modeling Earth Systems and Environment* **2024**, *10*, 19–44. https://doi.org/10.1007/s40808-023-01835-x.
8. Aderyani, F.R.; Jamshid Mousavi, S.; Jafari, F. Short-term rainfall forecasting using machine learning-based approaches of PSO-SVR, LSTM and CNN. *Journal of Hydrology* **2022**, *614*, 128463. https://doi.org/https://doi.org/10.1016/j.jhydrol.2022.128463.
9. Nayak, G.; Alam, W.; Singh, K.; Avinash, G.; Ray, M.; Kumar, R.R. Modelling monthly rainfall of India through transformer-based deep learning architecture. *Modeling Earth Systems and Environment* **2024**, *10*, 3119–36. https://doi.org/10.1007/s40808-023-01944-7.
10. Li, W.; Liu, C.; Hu, C.; Niu, C.; Li, R.; Li, M.; Xu, Y.; Tian, L. Application of a hybrid algorithm of LSTM and Transformer based on random search optimization for improving rainfall-runoff simulation. *Scientific Reports* **2024**, *14*. https://doi.org/10.1038/s41598-024-62127-7.
11. Brunner, M.; Slater, L.; Tallaksen, L.; Clark, M. Challenges in modeling and predicting floods and droughts: a review. *WIREs Water* **2021**, *8*. https://doi.org/10.1002/wat2.1520.
12. Colston, J.M.; Ahmed, T.; Mahopo, C.; Kang, G.; Kosek, M.; de Sousa Junior, F.; Shrestha, P.S.; Svensen, E.; Turab, A.; Zaitchik, B. Evaluating meteorological data from weather stations, and from satellites and global models for a multi-site epidemiological study. *Environmental Research* **2018**, *165*, 91–109. https://doi.org/https://doi.org/10.1016/j.envres.2018.02.027.
13. Hewage, P.; Behera, A.; Trovati, M.; Pereira, E.; Ghahremani, M.; Palmieri, F.; Liu, Y. Temporal Convolutional Neural (TCN) Network for an Effective Weather Forecasting Using Time-Series Data from the Local Weather Station. *Soft Computing* **2020**, *24*, 16453–82. https://doi.org/10.1007/s00500-020-04954-0.
14. Moraux, A.; Dewitte, S.; Cornelis, B.; Munteanu, A. A Deep Learning Multimodal Method for Precipitation Estimation. *Remote Sensing* **2021**, *13*, 3278. https://doi.org/10.3390/rs13163278.
15. Wu, H.; Zhou, H.; Long, M.; Wang, J. Interpretable Weather Forecasting for Worldwide Stations with a Unified Deep Model. *Nature Machine Intelligence* **2023**, *5*. https://doi.org/10.1038/s42256-023-00667-9.
16. Foehn, A.; García Hernández, J.; Schaefli, B.; De Cesare, G. Spatial interpolation of precipitation from multiple rain gauge networks and weather radar data for operational applications in Alpine catchments. *Journal of Hydrology* **2018**, *563*, 1092–1110. https://doi.org/10.1038/s41598-024-62127-7.
17. Nag, P.; Sun, Y.; Reich, B.J. Spatio-temporal DeepKriging for interpolation and probabilistic forecasting. *Spatial Statistics* **2023**, *57*, 100773. https://doi.org/https://doi.org/10.1016/j.spasta.2023.100773.
18. Casolaro, A.; Capone, V.; Iannuzzo, G.; Camastra, F. Deep Learning for Time Series Forecasting: Advances and Open Problems. *Information* **2023**, *14*. https://doi.org/10.3390/info14110598.
19. Orozco López, E.; Kaplan, D.; Linhoss, A. Interpretable Transformer Neural Network Prediction of Diverse Environmental Time Series Using Weather Forecasts. *Water Resources Research* **2024**, *60*. https://doi.org/10.1029/2023WR036337.
20. Nie, T.; Qin, G.; Ma, W.; Mei, Y.; Sun, J. ImputeFormer: Low Rankness-Induced Transformers for Generalizable Spatiotemporal Imputation. In Proceedings of the Proceedings of the 30th ACM SIGKDD Conference on Knowledge Discovery and Data Mining, New York, NY, USA, 2024; KDD '24, p. 2260–2271. https://doi.org/10.1145/3637528.3671751.
21. Cholissodin, I.; Sutrisno. Prediction of Rainfall Using Improved Deep Learning with Particle Swarm Optimization. *TELKOMNIKA* **2020**, *18*, 1272–1281.
22. Rahman, A.; Abbas, S.; Gollapalli, M.; Ahmed, R.; Aftab, S.; Ahmad, M.; Khan, M.A.; Mosavi., A. Rainfall Prediction System Using Machine Learning Fusion for Smart Cities. *Sensors* **2022**, *22*, 3504.
23. Praveena, R.; et al. Prediction of Rainfall Analysis Using Logistic Regression and Support Vector Machine. *Journal of Physics: Conference Series* **2023**, *2466*, 012032.
24. Tuysuzoglu, G.; Birant, K.U.; Birant, D. Rainfall Prediction Using an Ensemble Machine Learning Model Based on K-Stars. *Sustainability* **2023**, *15*, 5889.
25. Asha, P.; et al. An Efficient Hybrid Machine Learning Classifier for Rainfall Prediction. *Journal of Physics: Conference Series* **2021**, *1770*, 012012.
26. Ishwarya, G.; Santhrupthi, M.B.; Shanthi, B.; Varsha, N. The Literature Survey on Rainfall Prediction Using Machine Learning Techniques. *International Research Journal of Modernization in Engineering and Technology and Science* **2021**, *3*, 1999–2003.
27. Abbot, J.; Marohasy, J. Application of Artificial Neural Networks to Forecasting Monthly Rainfall One Year in Advance for Locations Within the Murray Darling Basin, Australia. *International Journal of Sustainable Development and Planning* **2017**, *12*, 1282–1298.

 doi:10.20944/preprints202605.0877.v1

28. Kang, J.; et al. Prediction of Precipitation Based on Recurrent Neural Networks in Jingdezhen, China. *Atmosphere* **2020**, *11*, 246.
29. Poornima, S.; Pushpalatha, M.; Jana, R.B.; Patti, L.A. Rainfall Forecast and Drought Analysis for Recent and Forthcoming Years in India. *Water* **2023**, *15*, 592.
30. Barrera-Animas, A.Y.; et al. Rainfall Prediction: A Comparative Analysis of Modern Machine Learning Algorithms for Time-Series Forecasting. *Machine Learning with Applications* **2022**, *7*, 100204.
31. Chhetri, M.; Kumar, S.; Roy, P.P.; Kim, B.G. Deep BLSTM-GRU Model for Monthly Rainfall Prediction: A Case Study of Simtokha, Bhutan. *Remote Sensing* **2020**, *12*, 3174.
32. Cho, K.; van Merriënboer, B.; Gulcehre, C.; Bahdanau, D.; Bougares, F.; Schwenk, H.; Bengio, Y. Learning Phrase Representations using RNN Encoder–Decoder for Statistical Machine Translation. In Proceedings of the Proceedings of the 2014 Conference on Empirical Methods in Natural Language Processing (EMNLP); Moschitti, A.; Pang, B.; Daelemans, W., Eds., Doha, Qatar, oct 2014; pp. 1724–1734. https://doi.org/10.3115/v1/D14-1179.
33. Weesakul, U.; Santipanusopon, P. Deep Learning Neural Network: A Machine Learning Approach for Monthly Rainfall Forecast, Eastern Thailand. *Engineering and Applied Science Research* **2018**, *45*, 242–248.
34. Liu, Y.; Liu, S.; Chen, J. RLNformer: A Rainfall Levels Nowcasting Model Based on Conv1D_Transformer for the Northern Xinjiang Area of China. *Water* **2023**, *15*, 3650.
35. Shah, U.; Garg, S.; Sisodiya, N.; Dube, N.; Sharma, S. Rainfall Prediction: Accuracy Enhancement Using Machine Learning and Forecasting Techniques. In Proceedings of the Proceedings of the 5th International Conference on Parallel, Distributed and Grid Computing (PDGC), 2018, pp. 373–378.
36. Asha, P.; Jesudoss, A.; Mary, S.P.; Sandeep, K.V.S.; Vardhan, K.H. Rainfall Prediction Using Machine Learning and Deep Learning Algorithms. *International Journal of Recent Technology and Engineering* **2021**, *10*, 251–254.
37. Kyros, G.; et al. A Machine Learning Approach for Rainfall Nowcasting Using Numerical Model and Observational Data. *Environmental Sciences Proceedings* **2023**, *26*, 11.
38. Khan, M.I.; Maity, R. Hybrid Deep Learning Approach for Multi-Step-Ahead Daily Rainfall Prediction Using GCM Simulations. *IEEE Access* **2020**, *8*, 52770–52784.
39. Mohia, Y.; Absi, R.; Lazri, M.; Labadi, K.; Ouallouche, F.; Ameur, S. Quantitative Estimation of Rainfall from Remote Sensing Data Using Machine Learning Regression Models. *Hydrology* **2023**, *10*, 52.
40. Shi, X.; et al. Deep Learning for Precipitation Nowcasting: A Benchmark and a New Model. In Proceedings of the Proceedings of the 31st Conference on Neural Information Processing Systems (NeurIPS), 2017, pp. 5617–5627.
41. Kim, S.; Hong, S.; Joh, M.; Song, S. DeepRain: ConvLSTM Network for Precipitation Prediction Using Multi-Channel Radar Data. arXiv:1711.02316, 2017. November.
42. Zhang, C.J.; Wang, H.Y.; Zeng, J.; Ma, L.M.; Guan, L. Tiny-RainNet: A Deep CNN with Bi-Directional LSTM for Short-Term Rainfall Prediction. *Meteorological Applications* **2020**, *27*, e1956.
43. Pudashine, J.; Guyot, A.; Petitjean, F.; Pauwels, V.; Uijlenhoet, R. Deep Learning for an Improved Prediction of Rainfall Retrievals from Commercial Microwave Links. *Water Resources Research* **2020**, *56*, e2019WR026255.
44. Manandhar, S.; Dev, S.; Lee, Y.H.; Meng, Y.S.; Winkler, S. A Data-Driven Approach for Accurate Rainfall Prediction. *IEEE Transactions on Geoscience and Remote Sensing* **2019**, *57*, 9323–9331.
45. Frame, J.M.; et al. Deep Learning Rainfall–Runoff Predictions of Extreme Events. *Hydrology and Earth System Sciences* **2022**, *26*, 3377–3392.
46. Wang, D.; Zhang, Y.; Zhao, Y. LightGBM: An Effective miRNA Classification Method in Breast Cancer Patients. In Proceedings of the Proceedings of the 2017 International Conference on Computational Biology and Bioinformatics, New York, NY, USA, 2017; ICCBB '17, p. 7–11. https://doi.org/10.1145/3155077.3155079.
47. Vaswani, A.; Shazeer, N.; Parmar, N.; Uszkoreit, J.; Jones, L.; Gomez, A.N.; Kaiser, L.; Polosukhin, I. Attention is all you need. In Proceedings of the Proceedings of the 31st International Conference on Neural Information Processing Systems, Red Hook, NY, USA, 2017; NIPS'17, p. 6000–6010.
48. He, Y. BERT-CNN-BiLSTM: A Hybrid Deep Learning Model for Accurate Sentiment Analysis. In Proceedings of the 2023 IEEE 5th International Conference on Power, Intelligent Computing and Systems (ICPICS), 2023, pp. 921–926. https://doi.org/10.1109/ICPICS58376.2023.10235335.
49. Kim, S.; Lee, S.P. A BiLSTM–Transformer and 2D CNN Architecture for Emotion Recognition from Speech. *Electronics* **2023**, *12*. https://doi.org/10.3390/electronics12194034.

 doi:10.20944/preprints202605.0877.v1

50. Choudhary, A.; Arora, A. Assessment of bidirectional transformer encoder model and attention based bidirectional LSTM language models for fake news detection. *Journal of Retailing and Consumer Services* **2024**, *76*, 103545. https://doi.org/https://doi.org/10.1016/j.jretconser.2023.103545.
51. Bashir, T.; Wang, H.; Tahir, M.; Zhang, Y. Wind and solar power forecasting based on hybrid CNN-ABiLSTM, CNN-transformer-MLP models. *Renewable Energy* **2025**, *239*, 122055. https://doi.org/https://doi.org/10.1016/j.renene.2024.122055.
52. Climate Hazards Center. CHIRPS: Rainfall Estimates from Rain Gauge and Satellite Observations. https://www.chc.ucsb.edu/data/chirps, 2025. Accessed: 2025-05-23.